Development and characterization of a beam line for an achromatic focus for the wavelengths 1050 nm and 1576 nm

Kai Gamlin
kgamlin@ethz.ch

Supervisors :
David Holzapfel
Dr. Fabian Schmidt
Dr. Daniel Kienzler

July 1, 2024

Abstract

The implementation of quantum logic spectroscopy (QLS) protocols on ions in a Paul trap often relies on the use of multiple laser beams with significantly different wavelengths. These protocols require the spatial overlap of multiple laser beams, some of which must be focused on a single ion. In this experiment, H_2^+ is co-trapped with a $^9Be^+$ ion in a Paul trap [1], and uses a 1050 nm beam to drive a Raman transition which excites the shared motional states of both ions. The spectroscopy transition between rovibrational states ($\nu = 0, L = 0$) to ($\nu = 3, L = 2$) of H_2^+ is at a wavelength of 1576 nm. The overlap of the two beams is guaranteed by coupling both wavelengths into the same optical fiber. The remaining challenge is to focus both wavelengths with the same lens system after they are outcoupled from the same optical fiber. A four-lens system is presented that focuses the two wavelengths onto the ion trap, taking into account the experiment's constraints: a circular aperture of the heat shield and a 20 mm focal length lens at a fixed distance from the ion trap inside the vacuum chamber. The lens system was designed using the ray-tracing software Zemax. The lens system produced a satisfactory overlap of the foci of both wavelengths as displayed in figure 8. At one point in space the lens system focuses the beams down to a waist of 6.72 ± 0.16 µm and 8.29 ± 0.20 µm for 1050 nm and 1576 nm respectively, satisfying the experimental requirements. This report illustrates the simulation and designing process on a ray tracing software and discusses the chopper wheel method to measure beam spot sizes, in doing so presenting an alternative laser beam spot size measurement method when no CCD camera is available for a given wavelength.

Contents

1 Introduction

At its core, scientific theory relies on experimental verification. High-precision spectroscopy of the rovibrational transitions of H_2^+ is used to test theoretical predictions of quantum electrodynamics or to measure fundamental constants such as the electron-proton mass ratio [2]. H_2^+ is the simplest molecular system and therefore of great interest for precise theoretical calculations. A consequence of the homonuclear nature of H_2^+ is the absence of dipole-allowed transitions due to the absence of a dipole moment in the system, i.e. the charge center and the center of mass of the three-body system coincide. Precision measurements of hyperfine and rovibrational transitions of H_2^+ by direct laser excitation are difficult because their inherently long lifetimes limit the signal acquisition process. H_2^+ is trapped in a Paul trap where the first-order Doppler shift is eliminated by cooling the molecular ion to its motional ground state [1]. Quantum logic spectroscopy is used to probe excited states in the various hyperfine and rovibrational manifolds of H_2^+. By co-trapping a beryllium ion Be^+ alongside H_2^+, one can transfer the information of the state of H_2^+, via the shared modes of motion between Be^+ and H_2^+, to the state of the beryllium ion [3]. A 1050 nm laser is used to

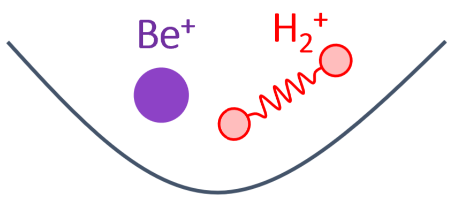

Figure 1: Sketch of the ion trap with Be^+ and H_2^+

drive a Raman transition coupled to the shared motional modes between the two ions and the internal electronic state of H_2^+. A 1576 nm laser is used to perform spectroscopy on the rovibrational transition from (ν =0, L =0) to (ν =3, L =2) in H_2^+. Both wavelengths must be focused on the molecular ion in the Paul trap. The restriction due to the limited number of viewing ports on the ultra-high vacuum chamber makes it preferable to find a solution with the same beam path for the 1050 nm and 1576 nm wavelengths.

Coupling both wavelengths into an optical fiber and focusing the outcoupled beam at the other end of the fiber would provide guaranteed beam front overlap and simultaneous focus on the trap. The alignment of the 1050 nm beam would guarantee the alignment of the 1576 nm beam. To implement this solution, one must find a combination of lenses that focus both wavelengths simultaneously. There is no trivial solution because most optics have wavelength-dependent focal lengths. In addition, achromatic lenses, which do not have this wavelength dependence, only work in certain wavelength ranges; 1050 nm and 1576 nm are too far apart for currently available commercial products. In addition, the short focal length lens mounted inside the vacuum chamber cannot be removed and would affect the focus of the two wavelengths even with a hypothetical achromatic lens.

The goal of this project is to design and build an optical path that focuses both wavelengths at the same point in space.

2 Theory and Simulation

This section introduces the principle of a ray tracing simulation, as well as various beam spot size metrics such as the root mean square (RMS) radius r_{RMS}, the airy radius, and the waist of a Gaussian beam.

2.1 Ray-tracing simulation

Geometric ray tracing assumes that the light beam of interest can be modeled as a large bundle of very narrow beams called rays. These rays are locally straight and perpendicular to the beam wavefront. The propagation of these rays is solved analytically using the Fresnel equations [4], which describe the behavior of planes at boundaries between different media. Note that this method does not take into account the wave nature of light. Any diffraction effects are not modeled by this simulation approach. The ray tracing simulation is performed using the Zemax Ansys software. The optical setup is described within the software by the boundaries, called surfaces, between different media. A surface can be described by its radius of curvature, material, coating, thickness and distance to the next surface, as well as other parameters for more complicated elements (e.g. non-plano-convex lenses). Several conditions on the beam path had to be met, in particular the last lens of the beam path is located inside the vacuum chamber at a distance of about 10 cm from the view port of the vacuum cell, with a heat shield in between with a numerical aperture in the form of a disk and a diameter of 4 mm.

The merit function editor was helpful in finding an optimal solution. This function minimizes a cost function that rewards smaller spot sizes in the image plane. Variables for this cost function can be defined by the user, e.g. the distance between surfaces or the radii of curvature of a surface boundary (i.e. a lens). The function then proceeds to minimize the root-mean-square radius value in the image plane (the last surface) by varying the values of the previously defined variables. This multi-variable optimization process can get stuck in local minima and converge to an unsatisfactory solution. The "Hammer Current" function is designed to force the optimizer to explore a different variable subspace and proved to be very helpful in finding the final solution. Figure 2(i) shows a 2D image of the optical beam path, where the light is out-coupled from a fiber collimator (F220APC-1310) on the left and focused on the image plane on the far right of the figure. Figure 2(ii) shows the table from the Zemax simulation software, in which each row describes a surface and each column describes a property of that surface, such as its thickness, radius of curvature, distance to the next surface, coating, and so on. The data shown in 2(ii) correspond to the data describing the lens layout shown in figure 2(i). Figure 3 displays the spot diagrams, i.e. the

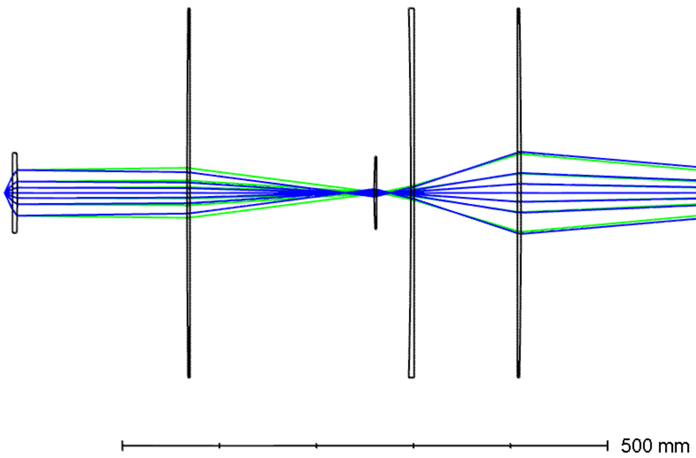

(i) Lens layout

	Surface Type	Comment	Radius	Thickness	Material	Coating	Clear Semi-Dia	Chip Zone	Mech Semi-Dia	Conic	TCE x 1E-6	Par 1(unused)	Par 2(unused)	Par 3(unused)
0	OBJECT Standard		Infinity	0.000			0.000	0.000	0.000	0.000	0.000			
1	Standard	F220APC-1310	Infinity	8.054			0.000	0.000	0.000	0.000	0.000			
2	STOP (a Standard		Infinity	5.032	D-ZK3M	THORC	2.750 U	0.000	2.750	0.000	-			
3	(aper) Even Asphere		-6.428	175.000		THORC	2.750 U	0.000	2.750	-0.731	0.000	0.000	-8.924E-05	-4.384E-07
4	(aper) Standard	LA4924-C	80.500	3.000	F_SILICA	AR	12.700 U	0.000	12.700	0.000	-			
5	(aper) Standard		Infinity	189.982 V			3.165 U	0.000	12.700	0.000	0.000			
6	(aper) Standard	LA4249-C	4.600	2.200	F_SILICA	AR	2.500 U	0.000	2.500	0.000	-			
7	(aper) Standard		Infinity	35.429 V			2.500 U	0.000	2.500	0.000	0.000			
8	(aper) Standard	LC1582-C	-38.590	3.500	N-BK7	THORC	12.700 U	0.000	12.700	0.000	-			
9	(aper) Standard		Infinity	106.429 V		THORC	12.700 U	0.000	12.700	0.000	0.000			
10	(aper) Standard	LA1986-C	Infinity	3.600	N-BK7	THORC	12.700 U	0.000	12.700	0.000	-			
11	(aper) Standard		-51.500	192.217 V			12.700 U	0.000	12.700	0.000	0.000			
12	Standard	40K shield	Infinity	10.254			2.000 U	0.000	2.000	0.000	0.000			
13	(aper) Standard	LA4194	9.200	2.000	F_SILICA		3.000 U	0.000	3.000	0.000	-			
14	(aper) Standard		Infinity	17.636			3.000 U	0.000	3.000	0.000	0.000			
15	IMAGE Standard		Infinity	-			6.130E-03	0.000	6.130E-03	0.000	0.000			

(ii) Lens data

Figure 2: Zemax simulation results for a given lens system. (i) Optical lens layout and ray-tracing simulation results for wavelengths 1050 nm and 1576 nm in blue and green, respectively. Note that the vertical scale is stretched by a factor of 15 with respect to the horizontal scale. The total length of the optical system from the fiber collimator to the focal point is about 741 mm. The distance between the fiber collimator and the first lens is highly adjustable and has a negligible effect on the relative distance between the remaining lenses. The distance between the first lens and the last lens is 547 mm. (ii) Zemax table of surfaces and their properties. The surfaces describe the lens layout from figure (i). All data in the table is taken directly from Thorlabs and their Zemax files with the corresponding product specifications.

intersections of the rays with the corresponding planes (heat shield plane and image plane).

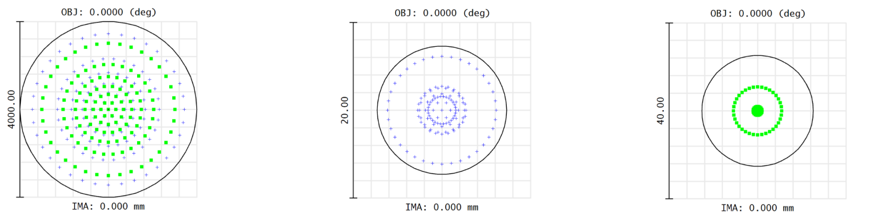

(i) heat shield plane **(ii)** image plane 1050 nm **(iii)** image plane 1576 nm

Figure 3: Spot diagrams of the beam path. Units are µm. The dots correspond to the intersections of rays with a given surface. Spots of 1050 nm and 1576 nm rays are shown in blue and green respectively. (i) Spot diagram for both wavelengths at the heat shield plane. The aperture of the heat shield is shown as the black circle. The beam must be contained within the aperture to avoid any clipping. (ii) Spot diagram at the image plane for the 1050 nm rays, the airy radius is shown as a black circle. (iii) Spot diagram at the image plane for the 1576 nm rays, the airy radius is shown as a black circle. A hexapolar ray distribution with ray density parameter of value 6 was used to create the spot diagrams

Table 1 summarizes the optical elements found using the simulation, namely their corresponding names from Thorlabs and their distance to one another. Note that the fiber collimator (FC) as well as the last lens of the system were imposed on the simulation. The last lens (L_5) is inside the vacuum chamber and cannot be modified.

Label of optical element	Thorlab Product	Distance to the next element [mm]
FC	F220APC-1310 (imposed)	175
L_1	LA4924-C	189.982
L_2	LA4249-C	35.429
L_3	LC1582-C	106.429
L_4	LA1986-C	202.471
		Distance to ion trap (fixed) [mm]
L_5	LA4194 (imposed)	17.636

Table 1: Summary of the different optical elements and their labelling for the rest of this report.

2.2 Beam spot size

There are several physical definitions to describe the spot size of a light beam. This subsection will focus on three, the Gaussian beam waist, the airy disk radius, and the root mean square (RMS) radius.

The Gaussian beam is defined as a solution of the paraxial Helmholtz equation. Only fundamental modes of Hermite-Gaussian beams are considered. The waist of a Gaussian beam w_0 is the radial distance from the axis of propagation to the point in space where the intensity has decreased by a factor of $\frac{1}{e^2}$ with respect to the maximum intensity. The airy disk corresponds to the smallest spot size in the focal plane of a perfect lens with a circular aperture illuminated by a beam of light with uniform intensity distribution. This spot size is a direct consequence of the diffraction of light at a circular aperture. Note that this definition of spot size requires a laser beam with a uniform intensity distribution, which is not the case when the lens system is illuminated by a Gaussian beam, i.e. a beam with a Gaussian intensity distribution of the wavefront. The root mean square radius of a beam propagating through a lens system is given by the following expression:

$$r_{\mathrm{RMS}} = \sqrt{\frac{1}{N}\sum_{N}^{i} R_i^2}, \tag{2.1}$$

with $R_i = [(x_i - x_o)^2 + (y_i - y_o)^2]^{1/2}$, where (x_i, y_i) are the coordinates of the intersection of the ith ray with the focal plane (i.e., the image plane) and (x_0, y_0) are the coordinates of the intersection of the chief ray with the focal plane. The system is said to be **diffraction limited** if the RMS radius is less than the airy disk radius.

The airy radius is calculated by propagating a beam of light with uniform intensity distribution through the lens system using Fourier optics. The RMS radius is calculated using equation 2.1 in the image plane. The Gaussian beam waist is calculated using the Physical Optics Propagation (POP) model. This model defines a Gaussian beam by an array of discrete sampled rays of the electric field. This array is complex valued and contains the phase and amplitude of the electric field in space. The physical optics propagation method allows a complete study of the properties of the beam, including diffraction effects caused, for example, by finite lens apertures. Table **??** summarizes the beam spot sizes of different wavelengths at the image plane calculated by Zemax.

	1576 nm	1050 nm
r_{RMS} [µm]	2.966	3.730
Airy Radius [µm]	10.96	7.3
waist w_0 [µm]	3.83	4.36

Table 2: Summary of the different beam spot size metrics given by Zemax for the optical lens system of Figure 2.

The waist w_0 is experimentally the quantity of interest because it is the one that is measured and compared to the simulation results. The quality of the optical lens system is characterized by the overlap of the foci of the two different wavelengths. The results for the airy radius and the RMS radius are still relevant because they show that the designed system is diffraction limited, which indicates that the system has reached its maximum resolution.

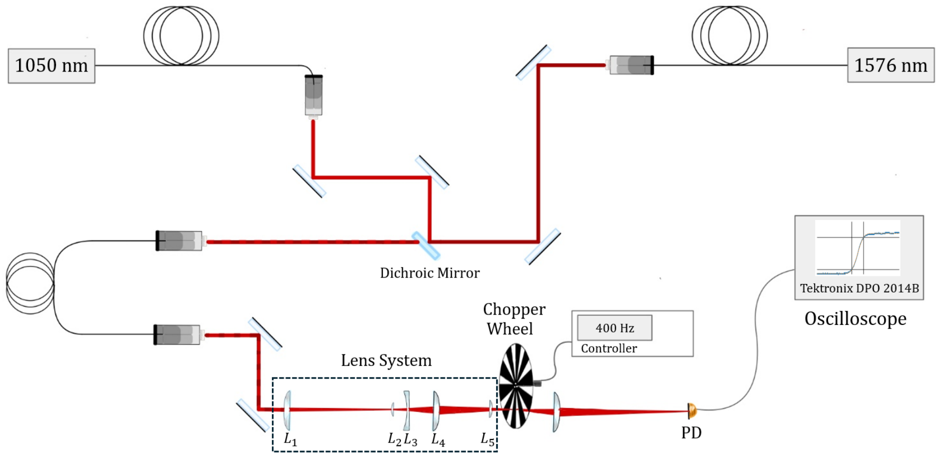

Figure 4: Sketch of the optical setup. The two different lasers beams are coupled into one fiber. For each wavelength two mirrors are used to adjust the four degrees of freedom for each beam to properly couple into the optical waveguide. The lens system is followed by a chopper wheel (MC1F10), whose frequency and phase is adjustable via a controller (MC2000B). The intensity of the light is recorded with photodiode (PD) (PDA05CF2). The modulation of the intensity due to the rotation of the chopper wheel is converted into an electrical voltage signal by the photodiode and recorded on an oscilloscope.

3 Experiment

This section describes the implementation of the lens system, its alignment, and the characterization of the beam spot size for the two different wavelengths using a chopper wheel and a photodiode.

3.1 Experimental Setup

Figure 4 shows a schematic overview of the optical setup that was built to test, align and characterize the lens system. The laser beams of wavelengths 1050 nm and 1576 nm are coupled into a polarization-maintaining fiber (P3-1064PM-FC-2) to ensure overlap of the beam fronts. A long-pass dichroic mirror (DLMLP1180) is used to combine the beam paths of the two different wavelengths before the fiber head. Once the two beams are coupled into the fiber, the two wavefronts overlap as they are outcoupled. The lens system is located immediately after the outcoupler, followed by a chopper wheel mounted on a translation stage. Finally, the light is focused onto a photodiode and the intensity is converted into a voltage signal.

3.2 Beam spot size characterization

This subsection aims to motivate why a chopper wheel was used over more common methods to measure spot size in the focal plane of the lens system. One could measure the spot size directly by placing a beam profiler (i.e., CCD camera) at the focal point, fitting a Gaussian profile to the observed intensity distribution, and determining the waist. However, CCD cameras that can detect wavelengths up to 1576 nm are rare. The research group did not have such a camera available. As an alternative, a knife-edge measurement was considered. This method looks at how the intensity of a photodiode voltage signal drops as a razor blade is raised through the focus. If the vertical position of the blade is known, the spot size can be determined. However, this method doesn't allow for fast scanning of the spot size along the axis of propagation, since a vertical scan must be performed at each position, the spot size calculated, and then compared to previous values.

Measuring with a chopper wheel is similar to measuring with a knife edge. The chopper wheel is inserted perpendicular to the laser beam in the plane where the beam waist is to be measured, in this case the plane of focus. Rotation of the wheel chops the laser beam at an adjustable frequency. This induces a modulation of the laser beam intensity on the photodiode, resulting in an oscillating square function at the output voltage of the photodiode. If one zooms in on the edges of this function, one observes a characteristic curve shape behavior similar to an error function. By determining the rise time of this function, and using some geometric considerations regarding the beam spot and the chopper wheel, one can determine an approximate value for the diameter of the beam spot size. Figure 5 shows the underlying principle that relates the rise time of the intensity signal to the spot size of the beam, as well as the geometric considerations required to mathematically relate these quantities. Equation 3.1 shows the relationship between the rise time from 10% to 90% of the measured intensity t_r, the distance of the laser spot to the center of the wheel R, and the rotation frequency of the wheel f_{rot}. The factor 1.56 is needed to compensate for the fact that the distance $R \cdot \theta(t_r)$ for a rise time from 10% to 90% of the integrated intensity is smaller than the Gaussian beam diameter.

$$D = 2w_0 \approx 1.56 \cdot (2\pi f_{\mathrm{rot}} t_{\mathrm{r}}) \cdot R. \tag{3.1}$$

Note that in the expression for the beam waist w_0 in equation 3.1, the rotation frequency of the wheel is involved, not the chopping frequency, which is the adjustable frequency. Their relation for a wheel of type MC1F10 is trivial, the wheel has ten covered disks, ergo to chop the beam at a

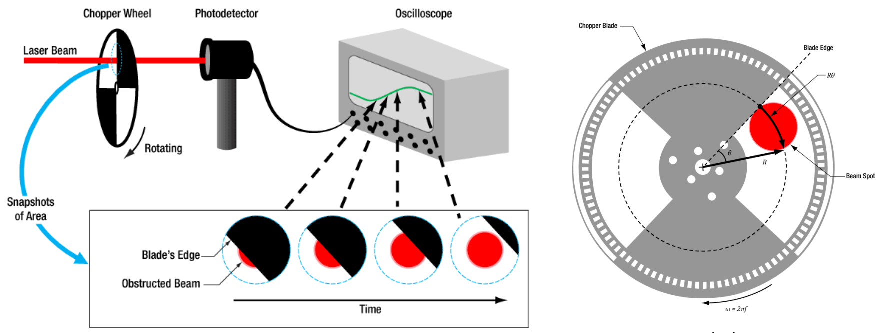

(i) (ii)

Figure 5: Sketch of the chopper wheel spot size measurement principle. Figure 5(i) sketches the principle of the rise time measurement and its relation to the spotsize. As the blade passes over the laser beam there is a gradual increase of the recorded intensity on the PD proportional to the integrated intensity distribution of the sections of the gaussian beam not blocked by the blade. Figure 5(ii) shows the geometrical motivation for equation 3.1. The approximation of the diameter to $R \cdot \theta$ is valid to first order for small spotsizes, i.e. small angles and $R \gg D$, both of which are true in the regime this method is used for here. Both picture were taken from Thorlabs.

frequency of 10 Hz, the wheel rotates at a frequency of 1 Hz.

$$f_{\text{rot}} = \frac{f_{\text{chop}}}{10}. \tag{3.2}$$

The rise time is directly proportional to the waist of the beam, so any change in the position of the wheel will cause a change in the waist value, ergo in the rise time seen on the oscilloscope, thus allowing a fast scanning method to qualitatively determine the plane of focus. The chopper wheel can be thought of as a device that performs 10 knife edge measurements in one rotation cycle.

Due to the short Rayleigh range, if the wheel is bent only a few tens of µm, different blades will cut the beam at different levels along the propagation axis. This effect is observed on the oscilloscope as an overlap of different error functions with longer and shorter rise times depending on the position of the wheel with respect to the focal point. Figure 6 shows an image of an oscilloscope display showing the rise time fluctuations. When recording a particular rise time data set on the oscilloscope, it is not clear from which blade it originates, so moving the wheel in increments of 10 µm and recording a second rise time data set does not guarantee that we are sampling the waist of the beam 10µm further.

Adding a delay to the oscilloscope trigger corresponding to just under one rotation period is sufficient to overcome this problem. If the rise time variations are caused by the different blades chopping the beam at different

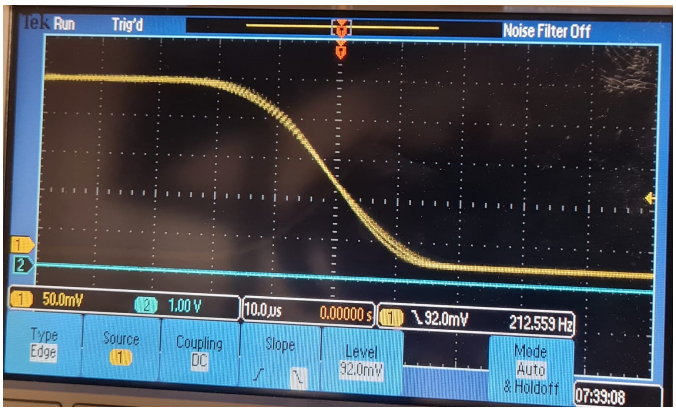

Figure 6: Oscilloscope display of fall time fluctuations, on the order of a few µs, cause an uncertainty of the order of tens of tens of µm.

points, the delay acts as a data selection corresponding to only one blade. No rise time fluctuations were observed after the trigger delay was implemented.

The characterization of the waist of the two different wavelengths was done using a chopping frequency of 400 Hz, i.e. a rotation frequency of 40 Hz. The frequency variation was deduced from the voltage square signal frequency variations observed on the oscilloscope. The maximum deviation from the chopping frequency was about 0.020 Hz, corresponding to an uncertainty of about 0.002 Hz on the rotation frequency. The laser beam is located at a distance of 4.2 ± 0.1 cm from the rotation axis of the wheel. Only one beam was scanned at a time for different longitudinal positions of the chopper wheel. When switching the laser beam wavelengths, it is crucial that there is an overlap of the two wavelengths on the photodiode before the first laser beam is blocked. This procedure ensures that we trigger the second wavelength with the same blade. Since there is no absolute frame of reference, it is necessary that both measurements are made with the same wavelength, otherwise there may be a significant systematic shift between the positions of the two wavelengths, making any statement about the positional overlap of the two foci in space sensitive to significant systematic uncertainties. In addition, there are other systematic effects if the selected blade is also tilted away from the perpendicular plane defined by the propagation axis; in such a scenario, the measured waists are overestimated because a larger cross section of the beam is examined. This systematic error is difficult to quantify with the setup used and is therefore not considered. Efforts were made to make sure that the wheel is perpendicular to the plane of propagation parallel to the optical table.

3.3 Experimental Results

The rise time curves for different chopper wheel positions was recorded onto an USB drive, and each curve was fitted with an error function of the form:

$$f_{\text{fit}}(t) = a \cdot (\text{erf}((t - b) \cdot d) + c). \tag{3.3}$$

Where a, b, c, d are variables to be fitted in order to best describe the curve shape behaviour. The fit of a given data set to equation 3.3 is performed using the *curve_fit* function from the *scipy.optimize* package. The 10% and 90% point are determined by finding the root of the following expression:

$$g(t) = f_{\text{fit}}(t) - (2p - 1 + c) \cdot a, \tag{3.4}$$

where p is the percentage of the intensity of the voltage signal (i.e. for 10% $p = 0.1$).

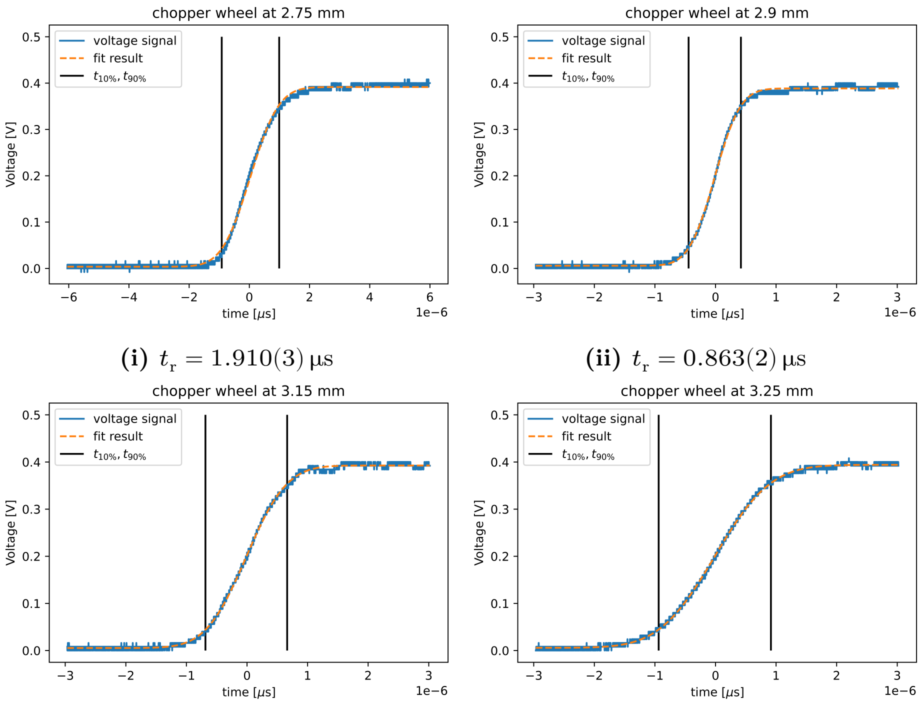

(i) $t_\text{r} = 1.910(3)\,\mu\text{s}$ **(ii)** $t_\text{r} = 0.863(2)\,\mu\text{s}$

(iii) $t_\text{r} = 0.817(2)\,\mu\text{s}$ **(iv)** $t_\text{r} = 1.349(2)\,\mu\text{s}$

Figure 7: Data recorded for different chopper wheel positions for the 1050 nm laser beam. The chopper wheel position indicated by the distance in the titles of the plots is a relative distance given by the handle of the translation stage on which the chopper wheel is mounted. The uncertainty of the rise time values corresponds to an upper bound on the standard deviation of these values. Details on the calculation of the rise time uncertainty can be found in the Python code.

Figure 7 shows 4 different voltage signals from the oscilloscope and their respective fits, as well as the determined rise times for the 1050 nm laser beam. Once the rise times are calculated, an estimate of the beam waist size can be determined using equation 3.1 and solving for w_0. The optical mount of the last lens prevents any absolute measurement between the last lens surface and the chopper wheel, making any statement about the absolute positions of the foci of the wavelength with respect to the last surface difficult in this configuration. Figure 8 shows that the foci of the two different wavelengths are spatially close, e.g. at a relative position of the chopper wheel of 3.05 mm the waist of the two beams, 6.72 ± 0.16 µm and 8.29 ± 0.20 µm for 1050 nm and 1576 nm respectively, meet the requirements of the experiment. The error bars in figure 8 do not take into account the fact that equation 3.1 is an approximation and inherits a certain uncertainty. They are only obtained by propagating the uncertainty of f_{rot}, t_r and R.

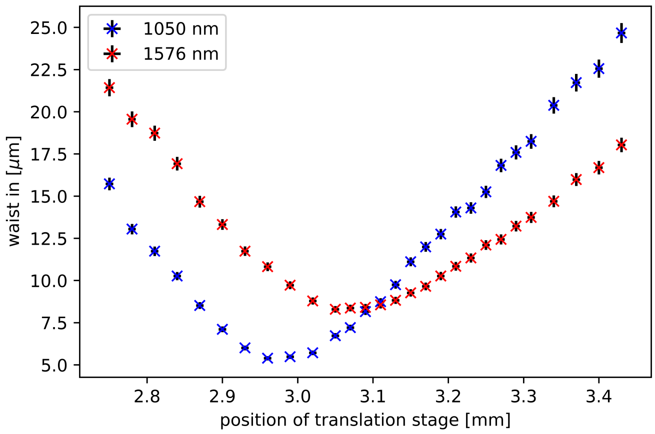

Figure 8: Waist of the two laser beams plotted against the relative position of the chopper wheel on a translation stage. The error bars of the waist values are about one to two order of magnitude smaller relative to their waist value

An accurate comparison between the lens distances given by the ray tracing simulation, as shown in table 1, and the actual distances between the lenses is difficult. Accurate length measurement of the distance between the surfaces of the lenses was hampered by the optical mounts, which block the lenses from all sides outside the lens system, and by the lack of instrumentation to measure these distances from within the beam path. The initial alignment used the distances given in table 1. Optimization of this alignment was attempted by estimating whether the distances between the lenses were above or below those given in table 1. This estimation still suffers from the length measurement problem mentioned above. To properly optimize the alignment, it would be necessary to modify the system and perform a similar waist scan as shown in Figure 8. Once this waist measurement is performed, one would compare the foci overlap and size between two alignments and implement or undo the change. This has not been done due to the large number of variables available and the time consuming nature of the waist measurement scans. The current alignment is not yet able to focus the two wavelengths as tightly as the simulation results for the beam waist from table 2 would suggest. This indicates that there is room for further improvement in the alignment of the lens system.

3.4 Challenges

The initial alignment of the beam with respect to the lenses was very sensitive to height mismatches between the laser beam and the center of the lens system. It was useful to get the exact height of the mounts to an accuracy of 0.1 mm from the CAD files provided by Thorlabs. This is a consequence of the fact that the lenses L_2 and L_5 have a diameter of 5 mm and 6 mm respectively; if the beam is a fraction of a millimeter away from the center of the lens, it is already significantly deflected. The two mirrors in front of the lens system, as shown in Figure 4, were instrumental in aligning the laser beam to the center of the lenses. The alignment of L_5 was made possible by the use of an x, y translation mount. Lenses L_1, L_2 and L_3 were mounted in an optical cage with L_2 and L_3 mounted in a z translation stage. L_4 was also mounted separately on a z translation stage.

Another challenge was the behavior of the square function at its edges. Not every rising curve followed a well-behaved error function model from Figure 7 as shown in Figure 9. Such curves affect the quality of the fit function due to their significant deviations from a classical error function. These curve shapes were first observed in a power regime of light that saturated the photodiode, so that by lowering the power, the behavior of most of the unusual curve shapes disappeared. However, even when the photodiode was not saturated, smaller similar features were still observed as shown in figures 9(i) and 9(ii). These were removed by tuning the phase of the chopper wheel and thus selecting a different blade. This indicates that these curve shapes are most likely artifacts of the edge of the chopper wheel blades.

Other unexpected curve shape behaviors, such as the one shown in figure 9(iii), were due to mechanical vibrations of the chopper wheel mount. These curve shape behaviors disappeared by slightly tightening or loosening the screws of the translation stage where the chopper wheel is mounted.

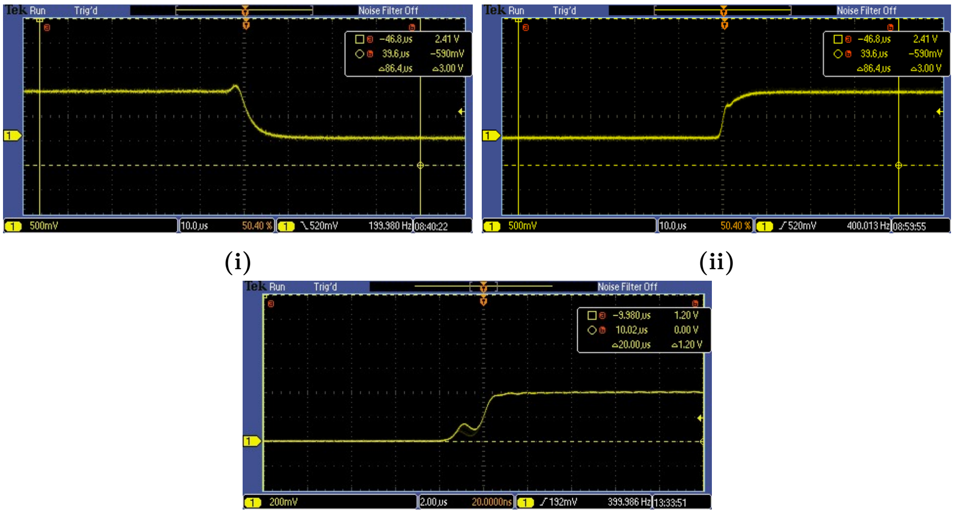

(i) (ii)

(iii)

Figure 9: Different rising voltage curves divergent from an expected error function curve behaviour. (i) & (ii) Rising voltage curves divergent behaviours possibly due to chopper wheel blade inhomogeneities. (iii) Rising voltage curve behaviour in the presence of mechanical vibrations of the chopper wheel system.

4 Conclusion

The goal of this project was to design and build an optical beam path that simultaneously focuses the wavelengths 1050 nm and 1576 nm using the same optics for both wavelengths coming out of the same optical waveguide. This ensures that the beam fronts of the two wavelengths overlap and simplifies the alignment of the two laser beams onto the ion. Using the ray tracing software Zemax, an optical system consisting of five lenses was designed, with the last lens located inside the vacuum chamber, which focuses both wavelengths at the same point in space at a fixed distance. The lens system was built and aligned to characterize the spatial overlap of the foci of the two different wavelengths. A sufficiently small focus, $6.72 \pm 0.16\,\mu\text{m}$ and $8.29 \pm 0.20\,\mu\text{m}$ for 1050 nm and 1576 nm respectively, was found for the purposes of the experiment, as can be seen in Figure 8. Two additional considerations to be made before transferring the lens system to the main experimental setup are, first, the influence of the glass of the vacuum window on the foci of the two wavelengths within the lens system. Second, the lens in the vacuum has been designed to have a tilt angle with respect to the vertical axis, which may have an influence on the lens system. Both considerations and their effects on the quality of the lens system can be simulated using ray tracing software. The lens system has been built using several z-translation stages, providing the possibility to tune and improve the system, thus ensuring a simplified implementation and alignment of the lens system to the main experiment.

References

[1] N. Schwegler, D. Holzapfel, M. Stadler, A. Mitjans, I. Sergachev, J. Home, and D. Kienzler, "Trapping and Ground-State Cooling of a Single H 2 +," *Physical Review Letters*, vol. 131, p. 133003, Sept. 2023.

[2] V. I. Korobov, L. Hilico, and J.-P. Karr, "Fundamental Transitions and Ionization Energies of the Hydrogen Molecular Ions with Few ppt Uncertainty," *Physical Review Letters*, vol. 118, p. 233001, June 2017.

[3] P. O. Schmidt, T. Rosenband, C. Langer, W. M. Itano, J. C. Bergquist, and D. J. Wineland, "Spectroscopy Using Quantum Logic," *Science*, vol. 309, pp. 749–752, July 2005.

[4] B. E. A. Saleh and M. C. Teich, *Fundamentals of Photonics*. Wiley, 1 ed., Aug. 1991.